Ca^{2+} sparks operated by membrane depolarization require isoform 3 ryanodine receptor channels in skeletal muscle

Sandrine Pouvreau*, Leandro Royer*, Jianxun Yi*, Gustavo Brum†, Gerhard Meissner‡, Eduardo Ríos*§, and Jingsong Zhou*§

*Section of Cellular Signaling, Department of Molecular Biophysics and Physiology, Rush University, 1750 West Harrison Street, Suite 1279JS, Chicago, IL 60612; †Departamento de Biofísica, Facultad de Medicina, Universidad de la República, Avenida General Flores 2125, Montevideo, Uruguay; and ‡Department of Biochemistry and Biophysics, University of North Carolina, Chapel Hill, NC 27599-7260

Communicated by Clara Franzini-Armstrong, University of Pennsylvania School of Medicine, Philadelphia, PA, January 29, 2007 (received for review October 3, 2006)

Stimuli are translated to intracellular calcium signals via opening of inositol trisphosphate receptor and ryanodine receptor (RyR) channels of the sarcoplasmic reticulum or endoplasmic reticulum. In cardiac and skeletal muscle of amphibians the stimulus is depolarization of the transverse tubular membrane, transduced by voltage sensors at tubular–sarcoplasmic reticulum junctions, and the unit signal is the Ca^{2+} spark, caused by concerted opening of multiple RyR channels. Mammalian muscles instead lose postnatally the ability to produce sparks, and they also lose RyR3, an isoform abundant in spark-producing skeletal muscles. What does it take for cells to respond to membrane depolarization with Ca^{2+} sparks? To answer this question we made skeletal muscles of adult mice expressing exogenous RyR3, demonstrated as immunoreactivity at triad junctions. These muscles showed abundant sparks upon depolarization. Sparks produced thusly were found to amplify the response to depolarization in a manner characteristic of Ca^{2+}-induced Ca^{2+} release processes. The amplification was particularly effective in responses to brief depolarizations, as in action potentials. We also induced expression of exogenous RyR1 or yellow fluorescent protein-tagged RyR1 in muscles of adult mice. In these, tag fluorescence was present at triad junctions. RyR1-transfected muscle lacked voltage-operated sparks. Therefore, the voltage-operated sparks phenotype is specific to the RyR3 isoform. Because RyR3 does not contact voltage sensors, their opening was probably activated by Ca^{2+}, secondarily to Ca^{2+} release through junctional RyR1. Physiologically voltage-controlled Ca^{2+} sparks thus require a voltage sensor, a master junctional RyR1 channel that provides trigger Ca^{2+}, and a slave parajunctional RyR3 cohort.

contractility | excitation–contraction coupling | sarcoplasmic reticulum

Cytosolic [Ca^{2+}] transients of excitable cells often require electrically initiated opening of ryanodine receptor (RyR) channels in the membrane of intracellular Ca^{2+} stores (1). Three isoforms of the RyR are controlled differently. In heart muscle RyR isoform 2 is activated by Ca^{2+} entering during the action potential [the calcium-induced calcium release (CICR) process] (2). In skeletal muscle and some neuronal terminals (3), RyR1 channels are opened by a mechanism that does not require Ca^{2+}entry (4) and involves dihydropyridine receptors (DHPRs), sensors of voltage V_m of the plasma and T membranes (5). The present study addresses the activation and roles of the third RyR isoform.

Different activation mechanisms result in different Ca^{2+} transients. Whereas in cardiac and frog skeletal muscle the V_m-elicited signals are composed of discrete events called Ca^{2+} sparks, which involve the concerted action of multiple channels (6–8), in mammalian muscle channels act individually, so that the responses lack sparks (9, 10). Nonmammalian skeletal muscles express two RyR isoforms: α, homologous to RyR1, and β (11, 12), homologous to RyR3 (13, 14). β and RyR3 have greater homology with RyR2 than RyR1. Isoform 3 is largely absent from adult mammalian muscle (15). Therefore, isoforms 3 or β are candidates for a crucial role in spark production. Here we establish the minimal molecular endowment for V_m-operated sparks.

Like the adult amphibian, the late mammalian embryo and the neonate have RyR1 and RyR3 and produce Ca^{2+} sparks. These sparks, however, are V_m-independent (16). Therefore, the mere presence of RyR1 or α and RyR3 or β is not sufficient for production of V_m-controlled sparks. The present work identifies additional requisites.

In all, there are three basic phenotypes of local Ca^{2+} signaling: (*i*) V_m-controlled transients devoid of sparks in adult mammalian muscle, (*ii*) V_m-controlled signals built from sparks in frog twitch muscle, and (*iii*) a duality of V_m-independent sparks and responses to V_m that lack sparks in the mammalian embryo. To understand how two RyR channel isoforms determine these functional phenotypes we endowed muscles of an adult mammal with RyR3. To tell whether the consequent functional changes were specific to isoform 3 we then caused expression of extra RyR1.

Results

Expression of Foreign Channel Proteins at High Density in Adult Muscle. Transfection was achieved by injecting plasmid vectors into the hind paws of adult mice and then electroporating the paw muscles by pulses applied through acupuncture needles (17). Shown in Fig. 1 *a* and *b* are fluorescence images of a paw and a flexor digitorum brevis (FDB) expressing GFP cDNA delivered this way. The images confirm the high efficiency of transfection achieved by this method. Fig. 1 *c* and *d* show yellow fluorescence, *F*, of a muscle transfected with rabbit RyR1 cDNA tagged with yellow fluorescent protein (YFP). The protein appears correctly targeted to the double row of junctions characteristic of mammals (see Fig. 1*i*). One of the nuclei in Fig. 1*c* (blue) is flanked by fusiform areas of high *F* (arrows), indicating high RyR synthesis in paranuclear endoplasmic reticulum (18). A second nucleus lacks high *F* regions, coinciding with lower *F* in sarco-

Author contributions: S.P., L.R., G.M., E.R., and J.Z. designed research; S.P., L.R., J.Y., G.B., E.R., and J.Z. performed research; G.M. contributed new reagents/analytic tools; J.Y. performed transformations and amplifications of DNA; S.P., L.R., G.B., G.M., E.R., and J.Z. analyzed data; and S.P., G.B., and E.R. wrote the paper.

The authors declare no conflict of interest.

Abbreviations: SR, sarcoplasmic reticulum; DHPR, dihydropyridine receptor; RyR, ryanodine receptor; CICR, calcium-induced calcium release; DICR, depolarization-induced calcium release; FDB, flexor digitorum brevis; YFP, yellow fluorescent protein.

§To whom correspondence may be addressed. E-mail: erios@rush.edu or jzhou1@rush.edu.

This article contains supporting information online at www.pnas.org/cgi/content/full/0700748104/DC1.

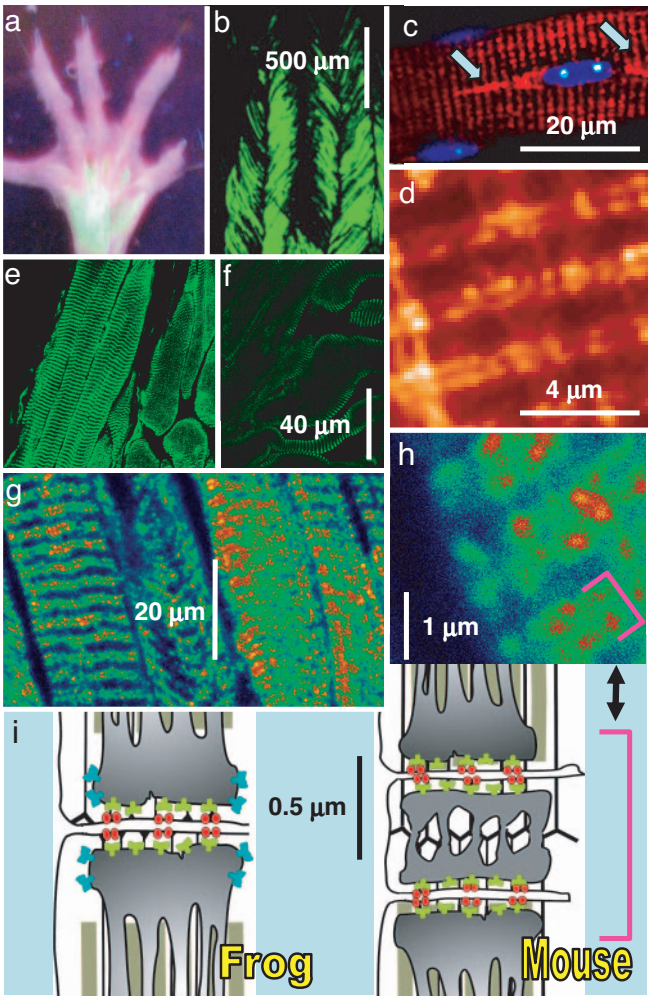

Fig. 1. Markers of expression in adult muscle. (*a* and *b*) Images of fluorescence from a mouse transfected with endoplasmic reticulum–GFP cDNA, showing expression in FDB and interosseus muscles (*a*) at efficiency close to 100% (*b*). (*c*) Overlay of confocal images of fluorescence of YFP (red) and blue fluorescence of a FDB fiber transfected with YFP-tagged RyR1 and stained with nuclear-selective Hoechst 33342. Arrows mark paranuclear areas of high YFP content. (*d*) YFP fluorescence at high magnification showing distribution in dual rows. (*e*) FDB transfected with RyR3 immunostained with anti-RyR3 Ab. (*f*) Immunostained control FDB. (*g* and *h*) FDB transfected and stained and at higher magnification to show doublets of stained rows. These rows correspond to triad junctions, as clarified by the diagram. (*i*) Location of triads and channels. In the mouse and other mammals there are two transverse tubules per sarcomere, located at the ends of the I band, so that two triads from neighboring sarcomeres (marked by the bracket) are close to each other; in amphibians, birds, and fish, a single triad is located at the center of the I band. DHPR (red) face RyR1 (green) in the T–SR junction. In nonmammals, RyR3 (blue) are located in the parajunctional SR membrane. The presence of doublets in the stained image (*d* and *h*, bracket) indicates that in transfected cells the foreign RyRs migrate to triads.

meres nearby. This segmental pattern of expression may be due to differences in transcribing activity at individual nuclei (19, 20). The other images are of muscles transfected with rabbit RyR3 (21). Immunolabeling with an antibody specific for RyR3 (22) shows immunoreactivity in transverse bands (Fig. 1*e*), which at higher magnification resolve into double rows of distinct foci (Fig. 1 *g* and *h*, bracket). As represented in Fig. 1*i Right*, in mammals one set of triadic junctions is present on each side of every Z disk, resulting in a doublet of closely placed triads (bracket). The staining therefore indicates that, like RyR1, RyR3 is targeted to triads, similar to RyR3 in muscles that natively

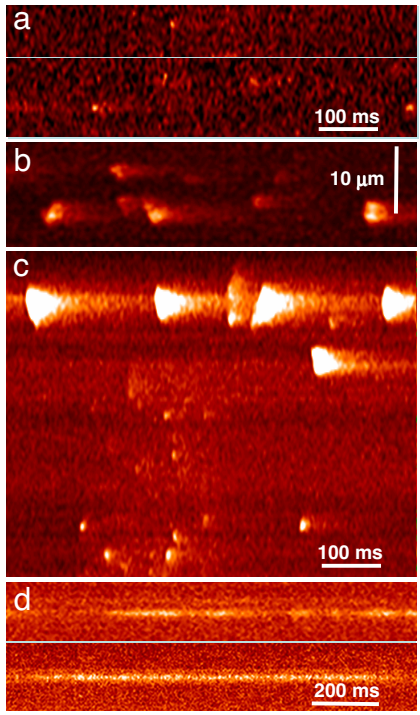

Fig. 2. Spontaneous events in fibers from transfected muscle. (*a*) Line scans in an intact fluo-4-loaded RyR3-transfected fiber featuring small sparks. (*b*) Intact fiber from another mouse showing large and more frequent sparks, sometimes propagating in space. (*c*) Variety of events in a RyR3-transfected cell voltage-clamped at −80 mV. Note large events near surface. (*d*) Line scans of fluo-4 fluorescence in two cells transfected with RyR1 and voltage-clamped. Note narrow Ca^{2+} ''embers.'' Line scanning was perpendicular to the fiber axis.

express the two isoforms (Fig. 1*i Left*). In nonmammalian muscle that natively contains two RyR isoforms, RyR3 is believed to occupy ''parajunctional'' positions, close to but not in contact with the junctional channels (23). This placement is consistent with the known inability of RyR3 channels to interact structurally (24) or functionally (25) with DHPRs. Moreover, for reasons of symmetry RyR3 molecules are more likely to form homomeric arrays than mix with RyR1 at the junction (23). For all of these reasons, foreign RyR3 (blue in Fig. 1*i*) presumably occupy parajunctional locations in these transfected FDB fibers. Although the YFP fluorescence and immunofluorescence images (Fig. 1 *d* and *h*) are not strictly comparable, the wider, more diffuse staining in Fig. 1*h* appears consistent with a parajunctional location of RyR3.

RyR3-Transfected Muscles Produce Ca^{2+} Sparks at Rest. Intact adult mammalian fibers at rest do not show Ca^{2+} sparks when stimulated (9). Spontaneous events are observed only upon membrane stress, deformation, or damage (26). By contrast, 30% of cells from muscles of 16 mice transfected with RyR3 exhibited discrete spontaneous events (Fig. 2 *a–c*). Some intact fibers showed brief events (Fig. 2*a*). Their properties, listed in Table 1, were similar to sparks of intact frog fibers (8). Other intact fibers gave wider events (Fig. 2*b*), many of which were sequentially propagating, similar to those seen in frogs in the presence of SO_4^{2-} (27, 28). Eleven RyR3 fibers that were patched and perfused exhibited a variety of events (as in Fig. 2*c*) including periodic ''macrosparks,'' wave-like events that usually originated near the fiber surface, at the ''high *F*'' nuclear flanking regions.

Ten percent of cells from muscles of six mice transfected with either RyR1 or YFP-RyR1 exhibited also events, but narrow and long-lasting (Fig. 2*d*), with average properties (Table 1) com-

Table 1. The discrete events of RyR-transfected cells

RyR	Amplitude	FWHM, μm	Rise time, ms	FDHM, ms	No. of events (cells)
RyR3, intact	1.51 ± 0.15	1.13 ± 0.11	7.97 ± 2.33	11.5 ± 2.62	23 (3)
RyR3, patch	0.56 ± 0.03	2.30 ± 0.09	17.9 ± 0.87	29.3 ± 1.29	85 (5)
RyR1	0.22 ± 0.01	2.26 ± 0.15	30.5 ± 3.20	54.8 ± 3.73	33 (3)

Events were detected automatically. Morphologic spark parameters are defined in *SI Materials and Methods*. All RyR1-transfected cells were patched and perfused with a solution containing 1 mM EGTA. RyR3 cells in the patched group included three cases with 1 mM EGTA and two cases with 5 mM EGTA in the pipette. FWHM, full width at half maximum; FDHM, full duration at half maximum.

parable with the "lone embers" of skinned mammalian fibers (28). Approximately 20% of RyR1-transfected cells exhibited large events (similar to the macrosparks in Fig. 2*c*), strictly localized near nuclei. Neither WT cells (Fig. 3 *a1* and *c1*) nor those transfected with other plasmids (endoplasmic reticulum–GFP, rabbit calsequestrin, and red protein-tagged calsequestrin silencer) displayed spontaneous events.

Ca^{2+} Sparks Respond to V_m Change in RyR3-Transfected Muscle. Clearly, expression of RyR3 endows adult fibers with Ca^{2+} sparks. But are these insensitive to membrane depolarization, like those of the embryo, or are they V_m-operated, as in the frog? We answered this question by imaging the response to either action potentials in intact fibers or V_m pulses under whole-cell patch clamp. In most of the transfected fibers, the $[Ca^{2+}]$ increase accompanying action potentials was large and fast, conditions that prevent the identification of sparks. Serendipitously, some RyR3-transfected cells responded to electrical stimulation with Ca^{2+} transients that were weaker than usual (probably because of partial depolarization of the plasma membrane), as shown in Fig. 4*a*. The action potential-mediated responses were composed of sparks. As shown by the profile in Fig. 4*f*, the spontaneous sparks, which were observed in 25 RyR3 fibers, often were larger, appeared near the surface and were independent of the electrical stimuli.

Exogenous RyRs crucially modified the response to voltage clamp. "Control" responses are in Fig. 3. In WT cells (Fig. 3 *a1–c1*) depolarizing pulses caused Ca^{2+} transients devoid of sparks, with a profile (black in Fig. 3 *a3–c3*) that increased during the pulse and dropped sharply afterward. This monotonic increase reflected a substantial steady level of Ca^{2+} release flux, sustained during the pulse. The release flux, derived from the Ca^{2+} transient, is plotted in Fig. 3 *a4–c4*. As reported earlier in experiments using photometry (29), the flux had an early peak, physiologically relevant, as it is representative of the activity elicited during the brief action potential of skeletal muscle. This peak was 2–2.5 times greater than the steady level reached immediately afterward (Fig. 3 *b4* and *c4*, black traces).

The response to V_m of RyR3-transfected cells is illustrated in Fig. 5. In Fig. 5*a Inset* is an *x–y* image of F/F_0 in the resting cell, showing a large wave "w" near a protruding nucleus. Spontaneous sparks, "s," which became frequent after the period of voltage stimulation used to generate the images in the figure, occurred only in the segment marked by the white bracket. Fig. 5 *a* and *b* shows responses to low V_m pulses, in scans along line AA in Fig. 5*a Inset*. Transients were largely constituted by sparks, of steeply V_m-dependent frequency. Responses at higher V_m, in a different cell, are in Fig. 5 *c* and *d*. Even though sparks, present at lower voltages, were no longer separable, there was a remarkable, qualitative difference with WT or RyR1 images at com-

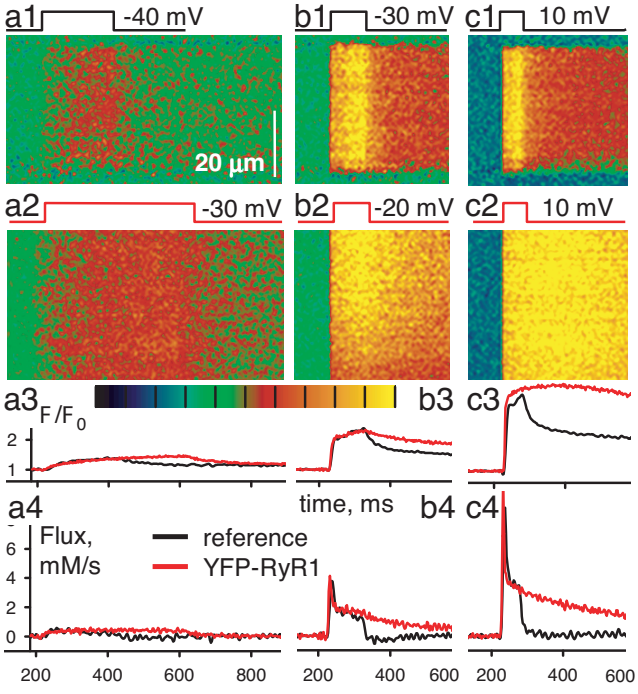

Fig. 3. Response to voltage clamp of WT and RyR1-transfected fibers. (*a1–c1*) Line scan images of $F(x,t)/F_0(x)$ in a WT fiber held at −80 mV and subjected to pulses represented at top. (*a2–c2*) Corresponding images in a YFP-RyR1-transfected cell. Black corresponds to $F/F_0 = 0$, and yellow corresponds to 2.5 (*a* and *b*) or 4 (*c*). (*a3–c3*) F/F_0 for WT (black) or RyR1 (red). (*a4–c4*) Ca^{2+} release flux derived from the image-averaged fluorescence using removal parameters fitted to the WT records.

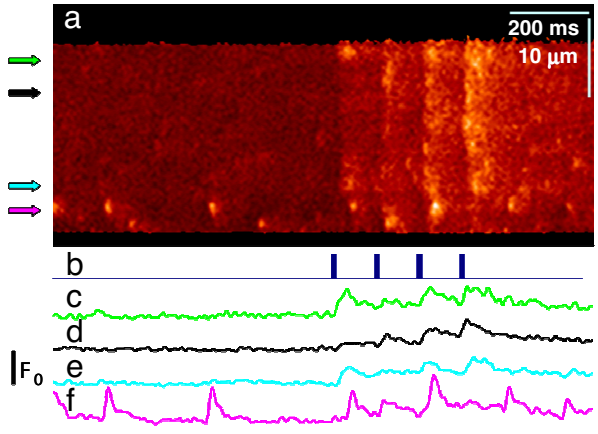

Fig. 4. Sparks activated by action potentials in RyR3-transfected muscle. (*a*) Line scan of a fiber from transfected FDB. The response to 0.5-ms field pulses (*b*) was composed of sparks. (*c–f*) Profiles of F/F_0 at arrows. Large sparks occurring spontaneously near the surface (lower edge of image and profile *f*) were unaffected by V_m.

PHYSIOLOGY

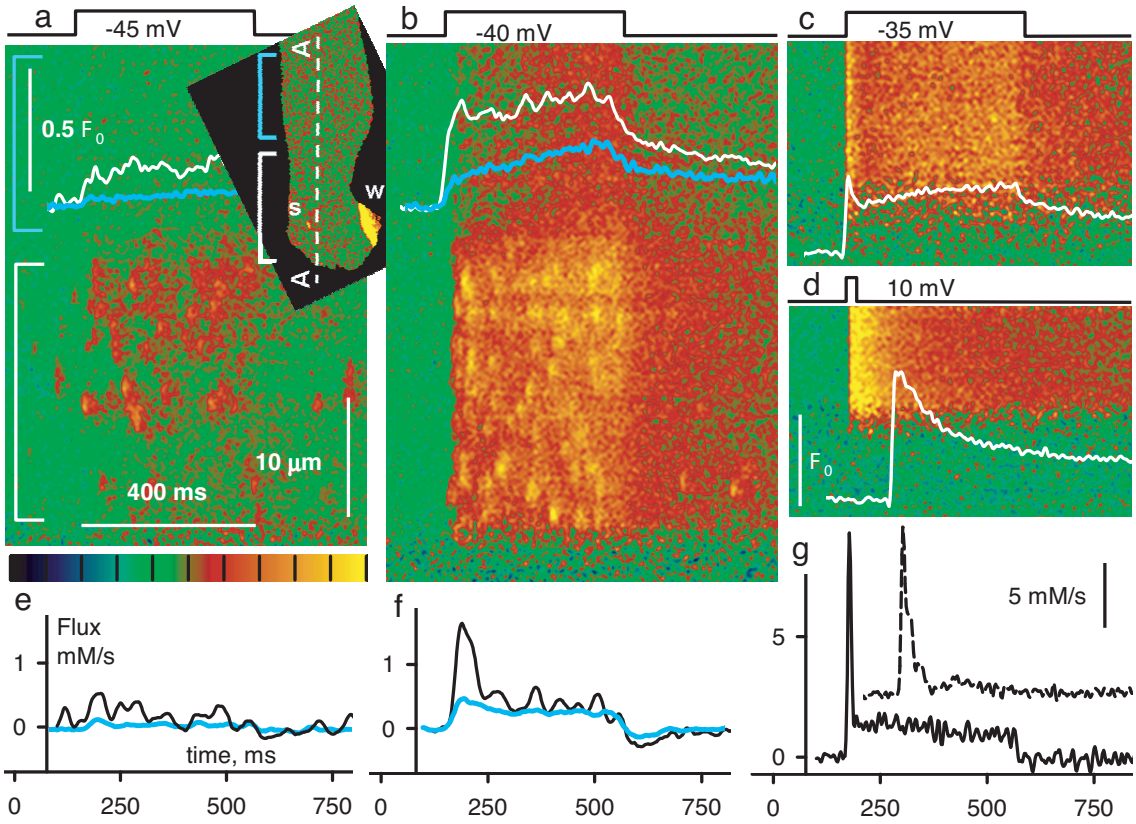

Fig. 5. Response to voltage clamp of RyR3-transfected fibers. (*a* and *b*) $F(x,t)/F_0(x)$ in scans along line AA of fiber in *Inset* showing responses to V_m. In the segment marked by the white bracket the response consisted largely of sparks. In the rest of the image (cyan bracket in *Inset* and *a*) the response was eventless, like that of WT muscle (Fig. 3*a1*). White and cyan traces plot F/F_0 averaged over x in the segments marked by color-matching brackets. (*c* and *d*) Responses to higher V_m in a second transfected cell. (*e* and *f*) Ca^{2+} release flux derived from the color-matched F/F_0 traces in *a* and *b*. (*g*) Release flux derived from traces in *c* (solid) or *d* (dashed; note scale and horizontal shift for visibility in records at 10 mV). Unlike the WT (Fig. 3 *b1* and *c1*), these responses show an early peak of fluorescence. Correspondingly, the peak in flux is more marked. Spatial scale is the same everywhere. Green in the color palette corresponds to $F/F_0 = 1$, and yellow corresponds to 2.5 (*a* and *b*) or 3 (*c* and *d*).

parable V_m; the evolution of fluorescence (plotted in white) had an early maximum rather than a monotonic rise.

To establish the isoform specificity of this change we examined the responses of fibers expressing foreign RyR1. Line scans of the responses to −30 mV (Fig. 3*a2*) or −20 mV (Fig. 3*b2*) are respectively similar to the WT responses to −40 or −30 mV (Fig. 3 *a1* and *b1*), a voltage shift observed in five of six fibers. Sparks were not present in the responses of RyR1-transfected cells. In conclusion, V_m-operated sparks require the presence of RyR3.

Unexpectedly, the decay in fluorescence after the pulses was much slower in the RyR1 transfectants (red traces) compared with the WT (black traces). The corresponding release flux (red in Fig. 3 *a4–c4*) seemed to terminate more slowly (Fig. 3*b4*) or not at all (Fig. 3*c4*). This anomaly was found in three of three YFP-RyR1 and three of three RyR1-transfected cells examined.

The Collective Effect of Ca^{2+} Release Built from Sparks. As can be seen in Fig. 5 *a* and *b*, only the 30-μm-long fiber segment within the white bracket produced sparks, spontaneous or in response to depolarization. In the adjacent region, bracketed in cyan in Fig. 5*a* and *Inset*, the response was synchronous with the pulse (indicating good voltage control) but it was of smaller amplitude and did not show distinct sparks. In this segment the response was indistinguishable from that of WT muscle at a comparable V_m (Fig. 3 *a1* and *b1*). Such segmental pattern of activity is probably due to transcription limited to individual nuclei (19, 20) (Fig. 1). The graphs in Fig. 5 *e* and *f* plot Ca^{2+} release flux derived from the Ca^{2+} transients in Fig. 5 *a* and *b* separately averaged over the two segments. At all voltages the flux in the segment with sparks (black trace) was much greater than in the area without sparks (cyan trace), which in turn was similar to that in reference or in RyR1-transfected fibers at a low V_m (Fig. 3). V_m-operated sparks therefore amplify release through RyR1, much as RyR2 amplify Ca^{2+} influx through L-type channels in cardiac muscle.

The amplification of Ca^{2+} release by sparks was greatest at the peak of the release flux waveform (as seen in Fig. 5 *f* and *g*), an effect that is best quantified through the peak/steady flux ratio, *p*/*s*. By this measure, the amplification of peak flux was most marked at intermediate V_m. For example at −35 mV (Fig. 5*g*) *p*/*s* reached a value of 7, while the corresponding value in the WT was ≈2 (Fig. 3*b*). Flux ratios in WT and transfected cells are compared in Fig. 6*a*. While the WT and RyR1 values (black or pink symbols) were mildly affected by voltage, *p*/*s* of transfected cells (red) was steeply V_m-dependent, with a prominent maximum at −35 mV.

Discussion

Ca^{2+} Sparks Controlled by Membrane Voltage Require Three Molecules. The initial phase of the response to an action potential in skeletal muscle is largely a function of two molecules. As depicted in Fig. 6*b*, transverse tubule membrane depolarization is translated by DHPRs to a conformational signal for RyR to open. In avian and mammalian muscle this so-called DICR

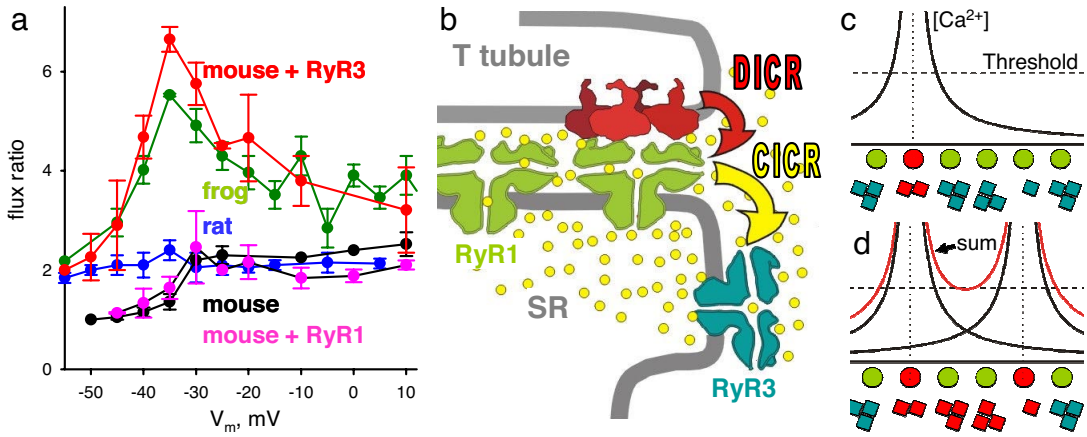

Fig. 6. Mechanisms of activation. (*a*) Ratio of peak over steady release flux vs. pulse voltage (V_m) in WT mouse (black, averages ± SEM, $n = 4$ fibers), RyR3-transfected fibers (red, $n = 11$ fibers and 8 mice), and YFP-RyR1 or RyR1 (pink, $n = 6$ fibers and 6 mice) compared with data from ref. 37 for rat EDL (blue) and frog semitendinosus (green). Note the similarity of frog and RyR3 mouse data. (*b*) A mechanism for V_m-operated sparks: T membrane depolarization is sensed by DHPRs (red), which activate underlying RyR1 by DICR. Ca^{2+} released through RyR1 then activates nearby RyR3, a CICR mechanism that may engulf a small cluster, to produce sparks. (*c* and *d*) The V_m dependence of amplification by CICR. Circles, junctional RyR1 operated by V_m; squares, RyR3 in parajunctional positions, assumed to open if local $[Ca^{2+}]$ rises above "threshold." At low V_m (*c*) only one RyR1 is activated (red). Curves are profiles of cytosolic $[Ca^{2+}]$; a cluster of RyR3 is activated by CICR (red). At higher V_m (*d*) two RyR1 channels are activated, but the number of open RyR3 channels (activated by the "sum" $[Ca^{2+}]$ profile) increases >2-fold. The diagram was modified from ref. 37.

mechanism (depolarization-induced calcium release) has a strict requirement for RyR1 as effector (25, 30, 31). Analogously, spark-like syntillas are activated by depolarization in hypothalamic nerve terminals [which express RyR1 (3, 32)] but are V_m-independent in mouse chromaffin cells, which lack this isoform (33).

What happens after RyR1 activation is unclear. As in the heart, V_m-operated Ca^{2+} sparks of frog skeletal muscle are believed to involve CICR (34); CICR should therefore contribute a large fraction of total Ca^{2+} release in frog cells, where the response is largely made of sparks. On the other hand, after carefully measuring Ca^{2+} release stimulated by applied Ca^{2+} in skinned frog fibers, Ogawa *et al.* (35) concluded that CICR makes a negligible contribution physiologically. We show here that introducing RyR3 into mammalian muscle recreates the frog phenotype, characterized by V_m-dependent sparks. From this observation it follows that RyR3 are required for the production of sparks physiologically operated by V_m. Because the present transfection places the RyR3 channels at the triad, their activation during V_m-operated sparks is probably triggered by Ca^{2+} released through RyR1. That the introduction of extra RyR1 molecules fails to reproduce the effect establishes V_m-operated sparks as a specific functional product of isoform 3.

We also showed that the physiologically relevant early peak in flux is potentiated by RyR3, which implies that CICR made a significant contribution to sarcoplasmic reticulum (SR) Ca^{2+} release in our RyR3-transfected cells. A similar component is probably present in native two-isoform cells.

The results are consistent with the three-molecule mechanism depicted in Fig. 6*b* whereby the initial DICR step is amplified, via CICR, by release through RyR3. This amplification enhances the concentration gradient that propels Ca^{2+} from release to target control sites on troponin C in areas where contractile filaments overlap. As illustrated in Fig. 1*i*, in nonmammalian species those sites are located farther away and are therefore harder to reach. A similar amplification by RyR3 of a primary Ca^{2+} signal (produced by $InsP_3$ receptors) may explain the contractile response of the pulmonary artery to hypoxia (36).

Amplification by CICR Has a "Signature." Both native two-isoform and RyR3-transfected muscles share a feature predicted for CICR. As illustrated in Fig. 5, the excess release in fibers transfected with RyR3 is greatest within the early peak of release flux, and the ratio of peak over steady flux is a sensitive measure of the effect. It is well known that this ratio differs sharply between frog and mammal (37). In Fig. 6*a* are plots of average ratios vs. V_m for frog (green symbols) and rat muscle (blue). *p/s* for the rat is lower at all voltages and quite constant. The frog values exhibit instead a steep nonlinear increase at low V_m and reach a maximum at intermediate voltages. There are obvious similarities between rat and WT or RyR1-transfected mouse ratios (black or pink) on one side, and frog and RyR3-transfected mouse ratios (red) on the other. The two systems containing RyR3 exhibit a signature mode at intermediate V_m.

A simple explanation of the V_m dependence [which updates a model of Shirokova *et al.* (37)] is presented in Fig. 6 *c* and *d*. V_m-operated RyR1 channels of the T-SR junction are depicted as a row of circles. Fig. 6*c* represents activation at a low V_m, which opens only one RyR1 channel in the group (red). The curves plot the profile of cytosolic $[Ca^{2+}]$ near the open channel. Among RyR3 channels located near the junction (squares) only those in the presence of a $[Ca^{2+}]$ above their activation threshold are open (red). At a higher V_m (Fig. 6*d*), addition of domains of elevated cytosolic $[Ca^{2+}]$ from two open RyR1 channels will lead to activation of RyR3 in numbers greater than the sum of those activated by the RyR1 opening individually. Therefore, at low V_m the gain provided by CICR over DICR will increase with voltage. At greater V_m the gain will decrease, because increasing DICR becomes proportionally less effective as a stimulus for CICR when most RyR3 are open. The recreation in a mammalian context, through addition of a Ca^{2+}-sensitive channel, of a response with quantitative features predicted by CICR, constitutes strong evidence of the involvement of CICR in these two-isoform systems.

Inactivation of Ca^{2+} Release and Termination of Sparks. As important for function as a rapid rise of the Ca^{2+} transient is its termination. This requires rapid restoration of the closed state of the RyRs, which in skeletal muscle is promoted by a Ca^{2+}-dependent inactivation process (38, 39). The preservation of the closed state at rest is assured by basal inhibitory effects of Mg^{2+} (40, 41) and various proteins (12, 42, 43). Large events occurring

spontaneously near nuclei in RyR1- or RyR3-transfected cells imply that newly synthesized channels spend more time open. By contrast, channels that have taken positions near junctions (as evidenced by their subordination to V_m) are stable, not opening until commanded by depolarization. Because basal inhibition works well for these channels, it must be associated with the interactions that enable control by V_m. Because this inhibition operates in transfected mice as well as in frogs, its mechanism must be fundamental, not dependent on species context. Stochastic attrition (44), the random turn-off of channels in a group, may be such mechanism. The effectiveness of attrition as an agent of event termination is steeply dependent on the size of the channel cluster (45). Because spontaneous events arise at arrays of newly synthesized RyRs, which must be extensive to support waves, attrition will affect them minimally; it should become increasingly effective as an inhibitory mechanism as these channels are dispersed in smaller clusters along triads in the SR.

Foreign RyR1 Channels Hinder the Response to V_m. The expression of foreign RyR1, YFP-tagged or not, failed to induce sparks but had two reproducible effects: a shift in the sensitivity to V_m and an apparent loss of the ability to rapidly terminate Ca^{2+} release upon repolarization. The demonstration of the second effect required an estimation of release flux, which relied on the assumption that "Ca^{2+} removal" properties and SR Ca^{2+} content remained unchanged. If this was not the case, then the anomalous "off" of the Ca^{2+} transients could have other explanations, for example a full depletion of Ca^{2+} in the SR during the pulses. In any case, impairment of control by V_m seems plausible upon incorporating slightly different and/or excessive channels to the junctional RyR1 lattice.

The efficient expression of a functional foreign channel protein, similar in density to that demonstrated for other proteins by DiFranco *et al.* (17), is unprecedented for adult muscle. As pointed out by these authors, the efficiency of this technique makes it suitable for the production of secreted proteins in gene therapy and structural and biochemical studies. The present success in reconstruction of a physiologically relevant signaling cascade portends a more systematic approach to structure-function studies, namely silencing of native proteins (46) combined with expression of their mutated substitutes plus genetically encoded, organelle-targeted sensors (47), in the cellular context of adult muscle.

Materials and Methods

All procedures and solutions are described in detail in supporting information (SI) *Materials and Methods*. Briefly, hind paws of adult mice were transfected as described in ref. 17. Animals were killed, and FDB were surgically removed ≈8 days later. Fibers were separated enzymatically and treated for immunohistochemistry as described in ref. 46. Voltage clamp was carried out with ≈0.8-MΩ pipettes containing a Cs glutamate-based solution. RyR1- or RyR3-transfected cells were identified by their spontaneous events after loading with fluo-4 AM. YFP-RyR1-transfected cells were identified by yellow fluorescence, then patched and loaded with X-rhod-2 through the pipette. Confocal imaging and derivation of $[Ca^{2+}]$ (t) and Ca^{2+} release flux were as described in refs. 10 and 37, respectively.

We thank M. DiFranco and J. L. Vergara (University of California, Los Angeles) for advice on the electrotransfer technique; S. R. Wayne Chen (University of Calgary, Calgary, AB, Canada) for the RyR3 plasmid; P. D. Allen (Harvard University, Cambridge, MA) for the YFP-RyR1; T. Murayama (Juntendo University, Tokyo, Japan) and V. Sorrentino (University of Milan, Milan, Italy) for anti-RyR antibodies; C. Franzini-Armstrong (University of Pennsylvania, Philadelphia, PA) for encouragement; J. Eu (Duke University, Durham, NC) for advice on immunostaining; X. Xu, Y. Chu, D. Santiago, and J. Tang (Rush University) for hands-on help, and T. DeCoursey (Rush University) for reading the manuscript. This work was supported by grants from Rush University (to J.Z.), Programa de Desarrollo de Las Ciencias Básicas de Uruguay (to G.B.), and National Institute of Arthritis and Musculoskeletal and Skin Diseases/National Institutes of Health (to G.M. and E.R).

1. Berridge MJ, Bootman MD, Roderick HL (2003) *Nat Rev Mol Cell Biol* 4:517–529.
2. Fabiato A (1983) *Am J Physiol* 245:C1–C14.
3. De Crescenzo V, ZhuGe R, Valazquez-Marrero C, Lifshitz LM, Custer E, Carmichael J, Lai FA, Tuft RA, Fogarty KE, Lemos JR, *et al.* (2004) *J Neurosci* 24:1226–1235.
4. Nakai J, Dirksen RT, Nguyen HT, Pessah IN, Beam KG, Allen PD (1996) *Nature* 380:72–75.
5. Ríos E, Brum G (1987) *Nature* 325:717–720.
6. Cheng H, Lederer WJ, Cannell MB (1993) *Science* 262:740–744.
7. Tsugorka A, Ríos E, Blatter LA (1995) *Science* 269:1723–1726.
8. Baylor SM (2005) *Cell Calcium* 37:513–530.
9. Shirokova N, Garcia J, Ríos E (1998) *J Physiol* 512:377–384.
10. Csernoch L, Zhou J, Stern MD, Brum G, Ríos E (2004) *J Physiol* 557:43–58.
11. Olivares EB, Tanksley SJ, Airey JA, Beck CF, Ouyang Y, Deerinck TJ, Ellisman MH, Sutko JL (1991) *Biophys J* 59:1153–1163.
12. Murayama T, Ogawa Y (1992) *J Biochem (Tokyo)* 112:514–522.
13. Giannini G, Clementi E, Ceci R, Marziali G, Sorrentino V (1992) *Science* 257:91–94.
14. Hakamata Y, Nakai J, Takeshima H, Imoto K (1992) *FEBS Lett* 312:229–235.
15. Sorrentino V (1995) *Adv Pharmacol* 33:67–90.
16. Shirokova N, Shirokov R, Rossi D, Gonzalez A, Kirsch WG, Garcia J, Sorrentino V, Ríos E (1999) *J Physiol* 521:483–495.
17. DiFranco M, Neco P, Capote J, Meera P, Vergara JL (2006) *Protein Expression Purif* 47:281–288.
18. Kaisto T, Metsikko, K (2003) *Exp Cell Res* 289:47–57.
19. Gussoni E, Blau HM, Kunkel LM (1997) *Nat Med* 3:970–977.
20. Vilquin JT, Kennel PF, Paturneau-Jouas M, Chapdelaine P, Boissel N, Delaere P, Tremblay JP, Scherman D, Fiszman MY, Schwartz K (2001) *Gene Ther* 8:1097–1107.
21. Chen SR, Li X, Ebisawa K, Zhang L (1997) *J Biol Chem* 272:24234–24246.
22. Kubota M, Narita K, Murayama T, Suzuki S, Soga S, Usukura J, Ogawa Y, Kuba K (2005) *Cell Calcium* 38:557–567.
23. Felder E, Franzini-Armstrong C (2002) *Proc Natl Acad Sci USA* 99:1695–1700.
24. Protasi F, Takekura H, Wang Y, Chen SR, Meissner G, Allen PD, Franzini-Armstrong C (2000) *Biophys J* 79:2494–2508.
25. Fessenden JD, Wang Y, Moore RA, Chen SR, Allen PD, Pessah IN (2000) *Biophys J* 79:2509–2525.
26. Wang X, Weisleder N, Collet C, Zhou J, Chu Y, Hirata Y, Zhao X, Pan Z, Brotto M, Cheng H, *et al.* (2005) *Nat Cell Biol* 7:525–530.
27. Zhou J, Brum G, Gonzalez A, Launikonis BS, Stern MD, Ríos E (2005) *J Gen Physiol* 126:301–309.
28. Zhou J, Brum G, Gonzalez A, Launikonis BS, Stern MD, Ríos E (2003) *J Gen Physiol* 122:95–114.
29. Ursu D, Schuhmeier RP, Melzer W (2005) *J Physiol* 562:347–365.
30. Airey JA, Deerinck TJ, Ellisman MH, Houenou LJ, Ivanenko A, Kenyon JL, McKemy DD, Sutko JL (1993) *Dev Dyn* 197:189–202.
31. Ward CW, Protasi F, Castillo D, Wang Y, Chen SR, Pessah IN, Allen PD, Schneider MF (2001) *Biophys J* 81:3216–3230.
32. De Crescenzo V, Fogarty KE, Zhuge R, Tuft RA, Lifshitz LM, Carmichael J, Bellve KD, Baker SP, Zissimopoulos S, Lai FA, *et al.* (2006) *J Neurosci* 26:7565–7574.
33. ZhuGe R, DeCrescenzo V, Sorrentino V, Lai FA, Tuft RA, Lifshitz LM, Lemos JR, Smith C, Fogarty KE, Walsh JV, Jr (2006) *Biophys J* 90:2027–2037.
34. Klein MG, Cheng H, Santana LF, Jiang YH, Lederer WJ, Schneider MF (1996) *Nature* 379:455–458.
35. Ogawa Y, Murayama T, Kurebayashi N (2002) *Front Biosci* 7:d1184–d1194.
36. Zheng YM, Wang QS, Rathore R, Zhang WH, Mazurkiewicz JE, Sorrentino V, Singer HA, Kotlikoff MI, Wang YX (2005) *J Gen Physiol* 125:427–440.
37. Shirokova N, Garcia J, Pizarro G, Ríos E (1996) *J Gen Physiol* 107:1–18.
38. Schneider MF, Simon BJ (1988) *J Physiol* 405:727–745.
39. Jong DS, Pape PC, Chandler WK, Baylor SM (1993) *J Gen Physiol* 102:333–370.
40. Meissner G, Darling E, Eveleth J (1986) *Biochemistry* 25:236–244.
41. Lamb GD (2002) *Front Biosci* 7:d834–d842.
42. Zhou J, Yi J, Launikonis BS, Royer L, Ríos E (2006) *Am J Physiol* 290:C539–C553.
43. Murayama T, Ogawa Y (2001) *J Biol Chem* 276:2953–2960.
44. Stern MD (1992) *Biophys J* 63:497–517.
45. Stern MD, Cheng H (2004) *Cell Calcium* 35:591–601.
46. Wang Y, Xu L, Duan H, Pasek DA, Eu JP, Meissner G (2006) *J Biol Chem* 281:15572–15581.
47. Rudolf R, Magalhaes PJ, Pozzan T (2006) *J Cell Biol* 173:187–193.